



HAL
open science

A new portable penetrometer for measuring the viscosity of active lava

M A Harris, S. Kolzenburg, I. Sonder, Oryaëlle Chevrel

► **To cite this version:**

M A Harris, S. Kolzenburg, I. Sonder, Oryaëlle Chevrel. A new portable penetrometer for measuring the viscosity of active lava. *Review of Scientific Instruments*, 2024, 95 (6), 065103 [14 p.]. 10.1063/5.0206776 . hal-04663298

HAL Id: hal-04663298

<https://hal.science/hal-04663298v1>

Submitted on 27 Jul 2024

HAL is a multi-disciplinary open access archive for the deposit and dissemination of scientific research documents, whether they are published or not. The documents may come from teaching and research institutions in France or abroad, or from public or private research centers.

L'archive ouverte pluridisciplinaire **HAL**, est destinée au dépôt et à la diffusion de documents scientifiques de niveau recherche, publiés ou non, émanant des établissements d'enseignement et de recherche français ou étrangers, des laboratoires publics ou privés.

A new portable penetrometer for measuring the viscosity of active lava

M.A. Harris^{1,a}, S. Kolzenburg¹, I. Sonder¹, M.O. Chevrel^{1,2,3,4}

¹*Department of Geology University at Buffalo, 126 Cooke Hall Buffalo, NY 14260-4130, USA*

²*Université Clermont Auvergne, CNRS, IRD, OPGC, Laboratoire Magmas et Volcans, 63000 Clermont-Ferrand, France.*

³*Université Paris Cité, Institut de physique du globe de Paris, CNRS, 75005 Paris, France*

⁴*Observatoire volcanologique du Piton de la Fournaise, Institut de physique du globe de Paris, 97418 La Plaine des Cafres, France*

a) Corresponding Author: martin.a.harris95@gmail.com

ABSTRACT

Viscosity is a fundamental physical property of lava that dictates style and rate of effusive transport. Studies of lava viscosity have predominantly focused on measuring re-melted rocks in the laboratory. While these measurements are well-constrained in temperature, shear rate, and oxygen fugacity, they cannot reproduce the complexities of the natural emplacement environment. Field viscosity measurements of active lava are the only way to fully capture lava's properties, but such measurements are scarce, largely due to a lack of easy-to-use, portable, and accurate measurement devices. Thus, there is a need for developing suitable field instruments to help bolster the understanding of lava. Here we present a new penetrometer capable of measuring a material's viscosity under the harsh conditions of natural lava emplacement. This device uses a stainless-steel tube with a semi-spherical tip fixed to a load cell that records axial force when pushed into a material, while simultaneously measuring the penetration depth via a free-moving tube that is pushed backward along the penetration tube. The device is portable (1.5 meters long, 5.5 kg in weight), and uses a single-board computer for data acquisition. The penetrometer has an operational range from 2.5×10^2 to 2.1×10^5 Pa s and was calibrated for viscosities ranging from 5.0×10^2 to 1.6×10^5 Pa s. It was deployed to the 2023 Litli-Hrútur eruption in Iceland. These field measurements successfully recorded the *in situ* viscosities of the lava in the range of 1.2×10^4 to 3.4×10^4 Pa s, showcasing it as an efficient method of measuring natural lava viscosity.

1 I. INTRODUCTION

2 For magmas, viscosity is a fundamental physical property that greatly influences their
3 transport and emplacement, such as ascent rates, effusion rates, and flow rates (Hon et al., 2003;
4 Kauahikaua et al., 2003; Cashman et al., 2013). In volcanic processes, the viscosity of silicate
5 melts can vary from $\sim 10^1$ - 10^{12} Pa s. This wide range in viscosity is predominantly due to variations
6 in the composition, temperature, volume of suspended solids, and exsolved fluid or gas phases.
7 Since lavas are three-phase mixtures containing melt, bubbles, and crystals, their bulk rheology is
8 directly linked to the volume fraction of each phase (Pinkerton and Stevenson, 1992; Harris and
9 Allen, 2008; Mader et al., 2013; Kolzenburg et al., 2022).

10 There have been numerous experimental, empirical, and analog investigations of lava
11 rheology that study different phase proportions in the mixture. This includes single-phase melts
12 (Shaw, 1969; Hess and Dingwell, 1996; Giordano and Dingwell, 2003; Giordano et al., 2008;
13 Hobiger et al., 2011), two-phase (melt+crystal) mixtures (Marsh, 1981; Pinkerton and Stevenson,
14 1992; Sato, 2005; Chevrel et al., 2015; Moitra and Gonnermann, 2015; Kolzenburg et al., 2019),
15 and two-phase (melt + bubble) mixtures (Llewellyn et al., 2002; Rust and Manga, 2002; Truby et
16 al., 2015). For high-viscosity rocks (felsic), several studies successfully investigated the
17 rheological properties with three phases (melt+liquid+gas) (Hess et al., 2007; Avard and
18 Whittington, 2012; Pistone et al., 2013; Heap et al., 2014; Dobson et al., 2020). However, due to
19 the time it takes to conduct experimental measurements on melted low-viscosity rocks (mafic) at
20 atmospheric pressure in the laboratory, all the volatiles are released. Thus, currently, the only
21 method capable of measuring natural three-phase mafic lava viscosities is to perform in situ
22 measurements on active flows (e.g., Chevrel et al., 2018a, 2019, 2023).

23 To measure high-temperature lava properties on active volcanoes, it is essential to have
24 instruments that can withstand the temperatures present in natural lava flows, are portable, and
25 acquire data swiftly and accurately. These considerations have guided the development of the
26 instrument presented here. This new lava penetrometer has undergone comprehensive testing in
27 the laboratory and has gone beyond a proof-of-concept with its use at an active volcanic eruption
28 in Iceland, and shows durability and accurate results across a range of viscosities from 10^2 to 10^5
29 Pa s. Here, we present in detail the background, procedure, and capacity of this novel instrument
30 for measuring natural high-temperature lava viscosities.

31 II. BACKGROUND

32 2.1 Field Viscometry of Lava

33 Approaching active lava and conducting measurements requires bespoke instruments that
34 can withstand extreme conditions and yield accurate data. As a result, there are only twelve
35 published attempts at measuring active lava rheology (Einarsson, 1949, 1966; Shaw et al., 1968;
36 Gauthier, 1973; Pinkerton and Sparks, 1978; Panov et al., 1988; Keszthelyi, 1994; Pinkerton et al.,
37 1995b, 1995a; Pinkerton and Norton, 1995; Belousov and Belousova, 2018; Chevrel et al., 2018a,
38 2019).

39 Direct measurements of lava viscosity date back to 1949 (Einarsson, 1949). Early field
40 studies used crude instruments such as metal rods pushed into lava using body weight, while later
41 studies used motor-driven devices with electronic data acquisition systems. Prior work on field
42 viscometers shows that the results can be extremely useful in characterizing complex natural lava
43 rheology. For a more elaborate review see Chevrel et al., (2019) and the references therein.

44 Two categories of devices have proven useful in field rheology. Firstly, a penetration type,
45 that records the force needed to push a defined geometric shape into the lava. Secondly, a rotational
46 viscometer that records the torque and rotational speed of a shear vane immersed in the lava
47 (Chevrel et al., 2019). There are advantages and disadvantages to both methods, but overall, the
48 rotational viscometers are effective at low-viscosity ranges ($\sim 10^2$ - 10^4 Pa s) whereas the prior
49 penetrometers have been used in higher viscosity materials ($\sim 10^3$ - 10^6 Pa s). Recent advances in
50 rotational field viscometers are detailed in Chevrel et al., (2023).

51 2.2 Penetrometers

52 Penetrometers are scientific and industrial tools that have broad applications. The overall
53 concept of all penetrometers is to push a fixed geometric shape into a desired medium and record
54 the amount of force exerted to penetrate at a given rate or to a defined depth. The shapes of the
55 penetration head range from rounded, squared (or flat), conical, concave, and even mesh-webbing.
56 Within soil science, hand-held penetrometers are commonly conically tipped and used to assess
57 soil strength properties, often as a measure of Impulse (a change in momentum as Force \times time)
58 which in turn have implications for water content, soil density, drainage capacity, and root growth
59 availability (Herrick and Jones, 2002; De Moraes et al., 2014; Kirkham, 2014). The agricultural

60 penetrometers can be manually operated as static drivers pushed by an operator into the soil, or
61 driven with hydraulic pressure, and readouts are made with a loadcell and/or strain gauge. Other
62 approaches include dynamic methods that use the kinetic energy of known, freefalling masses to
63 drive a penetrating device into the soil (Herrick and Jones, 2002). Dynamic cone penetrometers
64 are also widely used in road and infrastructure engineering, where the strength of pavement is
65 relevant to road construction and maintenance (Boutet et al., 2011). Likewise, concrete condition-
66 assessing penetrometers are used to monitor the degradation of sewer systems that may need
67 restoration (Hall et al., 2022). Additionally, portable penetrometers are also developed by snow
68 scientists that investigate the strength of snowpack layers (Schneebeli and Johnson, 1998; Floyer
69 and Jamieson, 2010). Often these snow penetrometers are capable of measuring depths up to 1.5
70 m and are controlled via step-motors or manually guided through a platform into a snow layer of
71 interest. Lastly, industrial penetrometers are used for food quality control for rheological
72 consistency or overall material strength (Tanaka et al., 1971, 1972; Dubbelboer et al., 2018; Jantra
73 et al., 2018).

74 While many penetrometers already exist to measure a material's properties in the field,
75 they do not meet several criteria for *in-situ* measurements of lava (*i.e.*, a molten rock at a
76 temperature above 1000°C). The materials for such instruments need to be constructed out of high-
77 temperature resistive metals (*e.g.*, stainless steel). A lava penetrometer needs to be long enough
78 to safely reach and penetrate lava without the operator getting exposed to excessive heat (*i.e.*, 1.5-
79 2 m). Portability is also essential, as active lava environments are dynamic and volcanoes are hard
80 to predict. Thus, a lava penetrometer must be light so that it can be carried and moved swiftly by
81 one person if needed. The measurement procedure must also be efficient to limit exposure to high
82 temperatures, reduced oxygen conditions, noxious/acid gases, and dusty environments. Therefore,
83 self-contained electronic sensors are preferred and the use of external apparatus to set up the
84 measurements like a stand, tripod, or fixed rig is suboptimal. Lastly, while many other
85 penetrometers focus on the force-derived strength of compressible solids (*i.e.*, soil), for lava
86 investigations we seek the viscosity (*i.e.*, strain–rate–stress relationship) of an incompressible
87 liquid. Thus, simultaneous acquisition of force and displacement rate is needed (see discussion
88 below). These criteria have led some past volcanologists to design lava penetrometers for field use
89 (Einarsson, 1949; Pinkerton and Sparks, 1978; Panov et al., 1988; Belousov and Belousova, 2018,

90 Gauthier 1973). A summary of the three main types of lava penetrometers used in field studies is
91 presented below.

92 2.2.1 Mechanics of Existing Field Penetrometers for Lava Viscometry

93 1) A simple rod with a semi-spherical head is inserted into lava, and viscosity is estimated
94 from the force used to insert at a given rate (Einarsson, 1949; Pinkerton and Sparks, 1978; Panov
95 et al., 1988; Belousov and Belousova, 2018). This method relies on the assumption that the
96 potential effect of lava sticking to the rod is negligible and thus calculates viscous drag based on
97 Stokes' Law (*i.e.*, falling sphere viscometry).

98 2) A “ballistic” spear is shot at high (presumed constant) speed into lava. The viscosity is
99 determined via calibration of the depth of penetration in known standard liquids. Gauthier (1973)
100 employed this method on lavas from Mount Etna in 1971, to overcome limitations that simple
101 penetrometers experience as the lava cools around it during slow penetration. However, this
102 method encounters major limitations as it penetrates the outer crust before reaching the interior
103 lava. The distance of penetration depends on the combined resistance forces caused by the outer
104 crust and interior lavas. The result is an average viscosity measurement over the viscosity gradient
105 from the outer, cooler, almost solid crust to the hot, molten liquid (Gauthier, 1973). Also, the path
106 of the arrow before penetration varies every time so the kinetic energy available for penetration
107 varies, making the standard liquid calibration unprecise. Finally, it is unclear whether the strain
108 rates induced in the crust allow the lava to remain in the viscous relaxation field or whether it
109 pushes it into the elastic regime (Alidibirov and Dingwell, 1996).

110 3) An encased spring-loaded, piston-driven device, deployed by Pinkerton and Sparks
111 (1978) on Etnean lavas. The device is preheated and inserted through the crust before the piston is
112 activated, thereby overcoming the crust-forming limitations of the prior two device types.
113 However, the use of a piston device still encounters issues as the spring does not fully expand all
114 the way each time, which yields inconsistencies in the measurements (Pinkerton, 1978).
115 Additionally, the casing for the piston introduces a large volume of metal within the lava, thus
116 increasing the likelihood of large-scale quenching around the inserted device and thereby
117 influencing the rheological properties in the localized sampling area. Furthermore, the force is
118 dictated by the spring and thus the range of accessible viscosities is predetermined and low. Lastly,

119 the maximum possible piston penetration is ~ 9 cm, thus limiting the measurement within that
120 restricted depth (Pinkerton, 1978).

121 To summarize, prior penetration-type devices have employed various techniques that aim
122 to inform on the rheological properties of natural lava. However, some methods have resulted in
123 only qualitative data that is difficult to pair with higher precision results obtained from rheological
124 studies in the laboratory (*e.g.*, Einarsson, 1949; Gauthier, 1973), and others were not suitable (or
125 calibrated) for a wide range of lava viscosities (*e.g.*, Pinkerton and Sparks, 1978; Panov et al.,
126 1988; Belousov and Belousova, 2018). Also, none of the prior devices can precisely characterize
127 lava crust thickness because their force and displacement determinations have remained
128 decoupled, posing a limitation on measuring the full viscous gradient of cooling lava. Finally, the
129 combination of field rheology and textural characterization that is required to tie rheological
130 parameters to the textural state of the multiphase suspension are absent for field-penetrometer
131 measurements.

132 The presented penetrometer instrument aims to fill these gaps with a particular focus on:

- 133 1. Optimization of the instrument's design and sensors to work best for the expected
134 (apparent) viscosity range for mafic lavas (*i.e.*, 10^2 - 10^5 Pa s during *in-situ* viscosity
135 measurements at active lava flows). This requires simultaneous recording of force and
136 displacement during penetration.
- 137 2. Improvement of the ease of operation and mobility so that such a device can be easily
138 deployed in the field with a high success rate of accurate lava viscosity measurement.
- 139 3. The use of standard mechanical and electronic parts and sensors which are available in
140 large enough numbers, so that costs can be lowered and individually replaced with an
141 alternative if necessary.
- 142 4. Extensive testing and calibration of each instrument variant (penetrator geometry), such
143 that results can be compared with datasets generated in high-temperature rotational
144 viscometry-based lab-scale measurements which typically work with re-melted material.
- 145 5. Open availability of all parts and plans of the instrument's design and data acquisition
146 code.

147

148 III. INSTRUMENT DESCRIPTION

149 The goal of our penetrometer device is to measure the force needed to penetrate a viscous
150 lava at a given rate (distance over time). To measure penetration force, we mount a force gauge
151 between a base element made of aluminum and a long tube made of stainless steel, the 'penetration
152 tube' (19 mm diameter, 1.65 mm wall thickness, 150 cm long) (Fig. 1A). The penetration tip, a
153 stainless-steel hemisphere (38.1 mm diameter) is mounted to the end of this tube. In theory, other
154 tip geometric shapes and sizes could be used but would require a separate set of calibrations (see
155 section below). The penetration tube was chosen over a rod to reduce the device's weight but retain
156 rigidity, and the tube also allows the steel tip to be slotted within or exchanged if it becomes
157 damaged. This tip is tapered with rounded edges on the back side (opposite to the direction of
158 penetration) to aid the extraction process when the measurement is complete. The overall diameter
159 of the tip is greater than that of the penetration tube, thus eliminating the effect of friction of lava
160 as the penetration tube moves into the medium. Linear bearings restrict the possible motion of the
161 penetration tube to the force sensor's relevant axis and fix it to the base element (Fig. 1B). The
162 linear bearings for the penetration tube were selected to optimize stability, not for maximum travel
163 speed. We use commercial hand-held size force gauges with three interchangeable options: capable
164 of reading forces up to 1000, 500, and 100 Newtons (N), respectively. The reported accuracy for
165 each gauge was ± 2.0 N, ± 1.0 N, and ± 0.2 N, respectively. The desired gauge is selected based on
166 the expected viscosity range that is encountered in the field to facilitate the most sensitive and
167 accurate measurement. The force gauge is wired to a Raspberry Pi (or equivalent single-board
168 computer (SBC)) through a USB serial port.

169 To measure displacement, a lightweight tube, the 'displacement tube', is mounted onto the
170 penetration tube, also using linear bearings (Fig. 1A). These bearings were selected to support high
171 travel speeds at low friction. Testing showed that for the targeted viscosity ranges these friction
172 forces are negligible to the acting penetration force. A reflecting metal disc is mounted to the
173 displacement tube (with a slotted bottom to fit around the diameter of the penetration tube) and
174 acts as a target for the laser time of flight distance sensor, which is fixed to the base element (Fig.
175 1B). As the penetration tube is pushed into the lava, the displacement tube, free-floating in the low
176 friction bearings, and capped with a flat steel washer (for increased surface area to avoid
177 penetration into the lava) is simultaneously displaced backward to the penetration depth. This
178 motion brings the reflective target towards the distance sensor that registers displacement within
179 the range of 50-400 (± 5) mm and is connected to the SBC via inter-integrated circuit (I2C) pins.

180 Both force and displacement sensors are read simultaneously every 100 ms. The raw data
181 is converted to Unicode (UTF-8) and SI units for Force (N) and displacement (mm) and then
182 written to permanent storage (SD card) of the SBC in a CSV-like (comma-separated values)
183 format. The program uses the SBC's real-time clock to control the main data acquisition loop.
184 Sensor check and acquisition control is realized with robust flip switches which can be handled in
185 a rough environment (see Supplementary Material (S)1 for details).

186 The force gauge, electrical box, penetration tube, and displacement tube all rest on a
187 stabilizing slotted extruded aluminum profile (Fig. 1B). The mass of the penetration tube exerts a
188 constant force on the force gauge, which depends on the angle to the vertical axis (zero in
189 horizontal, maximal in vertical position). Therefore, the force gauge can be tarred quickly at any
190 angle, and measurements do not need to be done only horizontally or vertically. It does, however,
191 require the operator in the field to maintain that angle. Random deviations from the angle, for
192 example, in rough field environments manifest themselves as analog noise in the force signal.
193 Below described field tests show, however, that this is a manageable problem.

194 Handles are attached within the slots of the stabilizing bar and adjusted to positions that
195 are comfortable for the operator's arm's length. We find that fixing one handle pointing down from
196 the stabilizing bar and one pointing out on the side offers optimal control and ease of use, yet the
197 choice can be made by each individual.

198 At 150 cm the penetrometer is a relatively long hand-operated instrument. To ease
199 transport, it can be disassembled into smaller pieces. Along the final third of the penetrometer tube
200 and displacement tube (region closest to the penetrometer tip), we have engineered quick-release
201 junctions held with steel cotter pins (Fig. 1B). The disassembly also has an aspect related to safety:
202 Though lava flows may not be the fastest known phenomenon of volcanic eruptions, the processes
203 involved are not controllable in any way by humans and the flow progress is still hard to predict.
204 It could therefore become necessary to leave the measurement location quickly. If the penetrometer
205 gets stuck in cooling lava that would mean having to decide in seconds whether or not to leave the
206 whole instrument. The ability to sacrifice only part of the instrument by quickly removing it
207 supports safe decision making in the field.

208 The entire suite of electronic sensors is powered with a portable power bank fixed to an
209 electrical box. Supplement (S)1 contains the full list of electronic parts and detailed custom-
210 machined parts can be found on the online repository (see link below).

211 The rough application environment and measurement durations of 2 to 15 seconds make a
212 fragile graphical computer screen-like display the wrong choice for this instrument. Instead, we
213 chose to install a bright LED based 4-Digit 7-Segment display, which informs the user with pre-
214 defined messages about the current state, and potentially not working sensors. This choice reduces
215 the SBC's power consumption and increases the battery life (see S1 for more details). It also means
216 that any data visualization, even for quality check only, must be done in a postprocessing step. We
217 created a set of Python scripts that help to quickly visualize and run a standardized analysis on raw
218 sensor records (see below). These are available together with the penetrometer software code at
219 https://github.com/LAVAPUBMH/Lava_Field_Penetrometer.

220 IV. DATA PROCESSING AND CALIBRATION

221 Both sets of programs, for data acquisition and data analysis (see online repository for most
222 current versions), were written in the Python scripting language because the resulting code is
223 relatively easy to understand for most users (*e.g.*, students, researchers, and scientists who are not
224 computer scientists) while it also runs on the somewhat less performant hardware of an SBC. Both
225 programs use the numpy library (Harris et al., 2020); the data acquisition program further depends
226 on several smaller libraries that enable communication with the sensors; the data analysis program
227 uses Matplotlib (Hunter, 2007) for data visualization and user interaction. All the dependencies
228 are published under open-source licenses.

229 We have created a data processing procedure with Python codes that allow standard data
230 analysis, (*i.e.*, retrieval of speed and force as well as the viscosity, for a person without
231 programming knowledge). Raw signals are plotted against time in a graphical user interface
232 (GUI). The relevant time window can then be selected using the pointer/mouse, which is realized
233 with Matplotlib's `SpanSelector` object. The relevant time window for viscosity measurement is
234 a plateau of stable (*i.e.* constant or flat) force and negative, constant displacement slope (Fig.
235 2A). The SpanSelector can be used as many times as necessary to extract the desired data (Fig.
236 2B). Ultimately, once the user is satisfied with the specific portion of the penetrometer run
237 selection, the code calculates the mean or moving-averaged (depending on user preference) force

238 (N) and displacement rate (m/s) (*e.g.*, Fig. 2C), which in turn can be used to calculate the
239 viscosity using Eq.1 or Eq. 2 (See below discussion). The viscosity can also be processed with a
240 moving average or left as raw calibrated values. Depending on the material that is measured, the
241 operator may wish to smooth the viscosity signal or not. Both options are available in the
242 processing code. Ultimately, the user can specify in the code what size window is desired to run
243 the smoothing moving average function. All these codes are available at
244 https://github.com/LAVAPUBMH/Lava_Field_Penetrrometer.

245 The current penetrometer has undergone calibration and testing in three analog materials.
246 One Newtonian viscosity standard oil, Cannon N190000, and two non-Newtonian materials,
247 Tryptone (a casein-derived protein gel) and SillyPutty™. First, we measured all three materials
248 with an Anton Paar concentric cylinder rheometer calibrated with Cannon Oils certified
249 (#1262.01) by the National Institute of Standards and Technology (NIST). The concentric
250 cylinder rheometer is equipped with a water bath casing that allows for temperature-controlled
251 viscosity measurements between 2 and 60 °C. The volume of the analog material in the
252 concentric cylinder was approximately 30 ml in each case. We developed temperature-dependent
253 viscosity models for each of the three materials from the concentric cylinder data conducted at
254 constant temperatures and used these models to interpolate target viscosities for the penetrometer
255 calibration (Fig. 3 and S2). For this, we use a Vogel-Fulcher-Tammann (VFT) (Vogel, 1921;
256 Fulcher, 1925) equation (*i.e.*, $\eta = \eta_0 \exp(-B/(T-T_0))$) to describe best the temperature dependence
257 of the measured internal standards. A fit of the models to measured viscosities yielded
258 correlation coefficients, $R^2 = 0.999$, 0.999 , and 0.997 for N190000, Tryptone, and SillyPutty™,
259 respectively (see S2). Calibration measurements were conducted at shear rates where non-
260 Newtonian behavior was negligible (*i.e.*, no shear thinning, or other such effects detected). For
261 N190000 the shear rate range was 0.555 - 6.940 s^{-1} , for Tryptone 0.027 - 0.055 s^{-1} , and for
262 SillyPutty™ 0.014 - 0.033 s^{-1} .

263 We then conducted measurements using our penetrometer for each of the three analog
264 materials across a temperature range of ~ 12 - $45 \text{ }^\circ\text{C}$. The temperatures were controlled with a heating
265 and cooling system plumbed into a 20 L water bath. Within the water bath, we placed the respective
266 analog materials ($\sim 1.5 \text{ L}$ of N190000, $\sim 6 \text{ L}$ of Tryptone, and $\sim 8 \text{ L}$ of SillyPutty™) in glass beakers.
267 Tryptone and Sillyputty were measured in 10L beakers with diameters of 225 mm, and the

268 N190000 oil was measured in a 2L beaker with a diameter of 130 mm. The penetrometer tip is
 269 38.1 mm in diameter. The effects of a finite container size can be neglected if the beaker radius to
 270 sphere radius > 5 (Macosko, 1994). For tryptone and Sillyputty, the relationship of the beaker to
 271 the ball radius is $112/19=5.9$. For N190000, the ratio is less than 5 ($67.5/19=3.6$), however, our
 272 recovered viscosity values are within acceptable uncertainty to the known values of the standard
 273 oil (see below discussion and Fig. 3). We hence deem any wall effect quite negligible. Before each
 274 measurement, we ensured the material had reached thermal equilibrium with the water bath by
 275 probing the material with a PT100 thermoprobe ($\pm 0.5^\circ\text{C}$).

276 In the studies of Panov et al., (1988) and Belousov and Belousova (2018), assumptions
 277 were made based on the hemispherical tip of the penetrometer to use a modified version of Stokes'
 278 Law (Eq. 1) for viscosity derivation as:

$$279 \quad \eta = \frac{F}{3\pi\nu R_{eff}} \quad \text{Eq. 1}$$

280 where η is viscosity, F is the force of penetration, ν is the speed of penetration, and R_{eff} is the
 281 effective radius of the rod. In past studies, force is typically recorded by a hand gauge, and velocity
 282 is measured by recording the time needed for penetration of the rod to a given depth (using video
 283 analysis or stopwatches), or simply timing the immersion between marked intervals on the rod
 284 manually (Panov, V.K et al., 1988; Belousov and Belousova, 2018). Although both Panov et al.,
 285 (1988) and Belousov and Belousova (2018) recovered rheological values in the expected range of
 286 basaltic lava, their data reduction approach (Eq. 1) was purely based on assumptions that a
 287 hemisphere could be dealt with by halving a factor related to sphere size in the viscous drag
 288 formula (*i.e.*, 3π) and was not tested for validity with analog materials or calibration of any sort.
 289 We initially processed all the penetrometer data using Eq. 1. However, the results from all three
 290 analog materials had poor fits with the known viscosity values of our reference materials (Fig. 3).
 291 We then applied the unmodified Stokes' Law (Eq. 2) and recovered a better fit to the model curve
 292 (Fig. 3):

$$293 \quad \eta = \frac{F}{6\pi\nu R_{eff}} \quad \text{Eq. 2}$$

294 Yet, Stokes' Law (Eq. 2) also results in an inaccurate determination of the measured material's
 295 viscosity, as there was still a significant deviation from the known viscosities, particularly the

296 N190000 ($124 \pm 32\%$ Pa s) and SillyPuttyTM ($14 \pm 7\%$ Pa s) (Fig. 3). This is likely since the
 297 penetrating geometry is a hemisphere and not a full sphere and thus, any drag effects on the back
 298 side of the sphere are that the Stokes' Law treatment relies on are absent.

299 We then looked to an alternative calibration procedure that modifies Stokes' Law in lieu
 300 of an empirical, force-to-penetration speed ratio (Ns/m) relationship to known viscosity. This
 301 method replaces the theoretically derived geometric constraints from a falling sphere and instead
 302 uses the signals of the force gauge and distance sensor and compares them with the viscosities of
 303 calibration materials measured in a standard concentric cylinder setup. Our results show that the
 304 force-to-displacement rate ratios (F/v) obtained with the penetrometer from the three calibration
 305 materials have linear relationships to the known viscosities of the respective materials. Thus, for
 306 the calibration, the basic assumption of a linear dependency between η and F/v is formulated

$$307 \quad \eta = \frac{F}{v} m + b \quad , \quad \text{Eq. 3}$$

308 where slope m replaces the fixed geometry factor $1/6\pi R$ in Equations 1 and 2, and offset b
 309 compensates an instrument threshold. The calibration was then done by fitting Eq. 3 to measured
 310 F/v values and reporting parameters m and b (Table 1). We do not apply any correction for
 311 buoyancy forces in this procedure as the expected maximum effect lies around 0.14 N for the
 312 lighter calibration oil (N190000) and 0.42 N for non-porous, molten lava (see S3). These values
 313 are well below the sensitivities of the deployed force gauges of 1-3 N.

314 We choose to employ linear regressions with an offset from the origin, b in Eq. 3, as they
 315 yield the best fit with the lowest deviation from the known viscosities. The offset is not caused by
 316 the calibration material behavior or the geometrical setup (liquid's container size or penetration
 317 head diameter). It is likely caused by the penetration rod linear bearings (low friction), which
 318 stabilize the relatively long instrument assembly. Results show that calibration turned out to be
 319 best when divided into two ranges separated by a force-to-rate ratio threshold $F/v = 2 \times 10^3$ Ns/m
 320 (Table 1). All values above this threshold (as obtained for Trypton and SillyPuttyTM) are treated
 321 as *high* F/v . Values equal to or below the threshold are treated as *low* F/v (obtained from
 322 N1900000). Calibration shows that the instrument is validated only for $F/v > 500$ Ns/m and values
 323 below this point are below the current instrument sensitivity.

324 Furthermore, the measured signals of force and displacement contain random noise, and
 325 thus, the calculated viscosities, as given by Equation 3, are sensitive to such noise. To address this
 326 factor, we smooth the data with a moving average function that does not touch the time base. For
 327 a series of discrete values A_i measured at evenly timed times, t_i , the average is:

$$328 \quad \bar{A}_i = \frac{1}{2N+1} \sum_{k=i-N}^{i+N} A_k \quad \text{Eq. 4}$$

329 Here A can be penetration force, displacement, or calibrated viscosity and N is an integer that
 330 determines the size of the averaging window, $2N + 1$. The averaging window must have an odd
 331 sample number so that it is centered around the index i . Moving averages (Eq. 4) were computed
 332 for the force and displacement signals. Velocity, v , was computed as the negative time derivative
 333 of the averaged distance, \bar{D} : $v = -d\bar{D}/dt$ (see S4 for details). The time derivative was
 334 approximated with the central difference scheme. The negative derivative is necessary because the
 335 distance (from the displacement sensor) decreases at a positive speed during measurement.

336 Overall, calibrated values lead to smaller deviations than the Stoke’s Law method (Fig. 3).
 337 We find that the calibrated results of the N190000 oil viscosity range have a mean deviation from
 338 the known viscosity of $9 \pm 6\%$ (number of measurements, $n = 10$). The calibrated results of the
 339 Tryptone and SillyPutty™ viscosity range have a mean deviation from the known viscosity of $4 \pm$
 340 4% ($n=19$) and $7 \pm 3\%$ ($n=10$), respectively

341

342 **Table 1:** Calibration constants for the two F/v ranges

	F/v (Ns/m)	m (1/m)	b (Pa s)
<i>low</i>	$\leq 2 \times 10^3$	2.5	-1112
<i>high</i>	$> 2 \times 10^3$	3.1	-1687

343

344 The penetrometer, when calibrated as outlined above, can accurately measure the viscosities of
 345 materials from 5.0×10^2 to 1.6×10^5 Pa s (Fig. 4). A catalog of our measured, known, and
 346 calibrated viscosities for the three analog materials can be found in S2. To accurately use Eq. 3
 347 to determine viscosity with this penetrometer, it is essential for each different force gauge or
 348 distance sensor to undergo this calibration procedure.

349 V. MEASUREMENTS OF ACTIVE LAVA: ICELAND 2023

350 The field instrument we present here is made for *in-situ* rheological characterization of
351 high-temperature material: *i.e.*, active lava flows. To assess the effectiveness of the newly
352 developed penetrometer device, we tested it at an active volcanic eruption. For this, we performed
353 measurements on a slowly moving ‘A‘ā lava front of the Litli-Hrútur 2023 eruption on the
354 Reykjanes Peninsula in Iceland (Fig. 5).

355 For field measurement, the ideal configuration involved two scientists: One carried and
356 operated the field viscometer and the other assisted in watching out with a water bucket for
357 quenching the lava if needed. Before any measurement we rested the penetrometer tip near the
358 incandescent lava to pre-heat the metal to avoid lava quenching on the instrument (Fig. 5C). In a
359 natural context, when the molten lava is exposed to the air, it forms a cooler outer crust. ‘A‘ā lavas
360 are blocky masses that periodically collapse and break apart as they advance over time. The access
361 to interior molten melt was not always successful, and some measurements encountered
362 impermeable crust or bumped into obscured fragments of crust within the interior of the lava.
363 Therefore, we repeated measurements across a small section of exposed lava (30 cm window, Fig.
364 5C) to assess the reproducibility of the potentially heterogeneous lava. This type of dynamic
365 measurement technique that acquires force and displacement simultaneously within a
366 heterogeneous lava area is only possible with the device presented here.

367 To start the measurement, we would focus on areas that had molten material available and
368 where the displacement tube could rest on an outer portion of the cooled crust (Fig. 6A). When
369 needed, we removed the cooler crust using a hammer or metal pole, so we could directly access
370 the molten interior. The operator would steadily push the penetrometer into the lava for ~20 cm
371 depth, over ~2 to 15 seconds (*e.g.*, Fig 6B and C). Once the maximum displacement was reached,
372 the penetrometer was extracted from the lava, typically leaving a hole the diameter of the stainless-
373 steel tip for a matter of seconds (*e.g.*, Fig 6D). If any lava had stuck to the penetrometer during
374 extraction, it would be collected from the quench bucket and cataloged as field samples linked to
375 the specific measurement. Additionally, thermal readings were conducted just after the viscosity
376 measurements at the same site using K-type thermocouples ($\pm 1^\circ\text{C}$). The quenched lava samples
377 were cataloged and brought back for textural and chemical analyses (see S5) and for further
378 geological studies. Despite the extreme conditions of temperatures up to $\sim 1200^\circ\text{C}$ and corrosive

379 gases (*e.g.*, H₂S), there was no degradation of any mechanical parts of the penetrometer, including
380 the repeatedly immersed penetrometer tube and tip.

381 Natural lava is much more heterogeneous than analog materials and prepared, re-melted
382 field samples used in the laboratory. Erupting lava often has viscosity gradients caused by crust
383 formation, temperature gradients, or channelized flow fields. These changes in viscosity can be
384 measured with the penetrometer in a single run if such changes are continuous and relatively slow,
385 such that the steady-state assumption of Stoke's law is approximately satisfied. Slow in this context
386 means that the change of viscosity causes either a change of measured force or penetration speed.
387 None of these changes must be caused by a 'sudden' change in the driving force (here the operator).
388 Furthermore, the viscosity gradient cannot be large enough to cause changes in inertial forces
389 around the penetrometer head. Overall, these conditions are typically satisfied if both measured
390 displacement and force profiles are smooth without major bumps.

391 In total, we performed nine penetrometer measurements within the 15 m wide and 3 m tall
392 lava front, and the results are shown in Figure 7. Runs 1-2 were done back-to-back, followed by a
393 break of ~30 minutes before runs 3-5 were conducted. Runs 6 to 9 were done 25 minutes later, and
394 just after a large block collapsed from the 'A'ā pile exposing a ~1.5 m window of molten interior.
395 The overall range of viscosities recovered from the measurements spanned 1.2×10^4 to 11.0×10^4
396 Pa s, with penetration depths between ~0.14 and 0.15 m (Fig. 7A). The viscosities shown with
397 depth (Fig. 7A) were processed with a moving average (Eq.4) window of nine. We observe in runs
398 2 to 4 heterogeneous viscosities with depth, with initially high and/or fluctuating viscosities,
399 followed by a rapid decrease and an eventual flattening of values towards the deeper parts of the
400 measurements. We interpret this as penetration through varying thicknesses of cooler crust and
401 eventually reaching the molten interior indicated by the latter stable viscosity readings. In contrast,
402 the viscosities from the other measurements do not record penetration of highly variable crust (*e.g.*,
403 lava was freshly exposed after a block collapsed), and instead remain stable across the penetration
404 (Fig. 7A). This highlights the ability of this new device to accurately characterize spatial variations
405 in viscosity over the penetration distance – a capability that no previous instrument that was used
406 on active lavas had. The temperatures of the molten interior revealed that the earlier and later runs
407 (Runs 1-2, Runs 6-9) had slightly higher temperatures than the middle runs (Runs 3-5).

408 We investigated the temperature-specific viscosity of each run by only processing the
409 stable viscosity regions from Figure 7A, as these are the areas that best represent the molten
410 interior. We find that the viscosity for the Iceland lavas at this location ranges from 1.2×10^4 Pa s
411 at 1152°C , to 1.8×10^4 Pa s at 1150°C , and to 3.4×10^4 Pa s at 1148°C (Fig. 7B). Overall, the ranges
412 of the ‘A‘ā lava measured with the penetrometer are within the expected magnitudes of basaltic
413 ‘A‘ā lava (Hon et al., 2003; Robert et al., 2014; Sehlke et al., 2014). The field tests highlight that
414 the device recovers accurate viscosity data and can track relatively small changes in viscosity over
415 a narrow temperature range at high temporal and spatial resolution.

416 VI. DISCUSSION

417 A. Advantages and limitations of the instrument

418 The penetrometer device has the potential to measure a viscosity range of $\sim 2.5 \times 10^2$ to
419 2.1×10^5 Pa s based on plausible field measurement constraints from the 10-500N force over
420 measurement timescales of 2-30s. We view anything outside this range as either being too small
421 in measurement duration for accurate processing or beyond the physical limits of most adult
422 operators. We have specifically calibrated the device to viscosity ranges from 5.0×10^2 to 1.6×10^5
423 Pa s. The stainless-steel penetration tube, displacement tube, and tips are capable of withstanding
424 temperatures up to 1200°C for moderate timescales (*i.e.*, minutes). The high-temperature
425 performance is highlighted by the successful use in volcanic settings, where no lava-submersed
426 parts of the penetrometer broke, bent, or were damaged over two weeks of field measurements.
427 The quick releases at the far end of the device (see Fig. 1) ensure that even if parts exposed to high
428 temperatures were to incur damage, they can quickly be exchanged with replacement parts without
429 needing to rebuild the entire device.

430 Additionally, the size (1.5 m length), and weight (~ 5.5 kg) of the penetrometer allow for
431 operation by a single person with ease, making it highly mobile. Furthermore, this new
432 penetrometer has self-contained electronic data acquisition for simultaneous force and
433 displacement rates during measurements, a characteristic that is novel in comparison to all other
434 penetrometers used for field lava rheology. All operations are done using only two switches, which
435 are designed to be easily operated single-handedly by the device operator even with thick gloves.
436 Lastly, the material costs of this penetrometer are quite low (see S1), making it an attainable
437 instrument for most research centers around the world.

438 In earlier versions of the prototype, we had a K-type thermocouple fed through the tip of
439 the penetrometer. However, extensive laboratory and field tests at high temperatures revealed that
440 the duration of penetrometer measurement is too short for a thermocouple to equilibrate with its
441 surroundings. Thus, we removed the thermocouple in the current device so that all the data
442 acquired yield high confidence. Since temperature information is an important component of lava
443 rheology, we suggest that separate temperature readings are done with a device that can withstand
444 long immersion timescales in material adjacent to where the penetrometer measurements are
445 completed. For our case, we used standard stainless-steel sheathed type K thermocouples.

446 Additionally, in contrast with a field rotational viscometer that increases and decreases
447 rotational speeds (Chevrel et al. 2023), the penetrometer presented here has no defined way of
448 varying the imposed strain rate throughout an individual measurement. This poses a limitation as
449 not all materials have linear stress-strain relations (*e.g.*, Bingham, Herschel Bulkley, *etc.*) like
450 natural lavas (Kolzenburg et al., 2022). To probe varying strain rates, the operator can attempt to
451 manually vary the force at which the penetrometer is pushed into the material on subsequent
452 measurements. However, in the application of volcanology, this systematic repetition may not
453 always be feasible in dynamic lava flow settings as sometimes only one measurement is possible
454 in one location.

455 Lastly, the current device has a limitation of measurement calibration for viscosities lower
456 than ~ 500 Pa s. It is possible that employing different force gauges with greater sensitivity to
457 compressive strain may yield better results at these lower viscosity ranges, but further testing
458 would be required to verify that approach. Alternatively, the combination with a rotational
459 viscometer able to measure viscosity within (10 to 650 Pa s; Chevrel et al. 2023) is suggested to
460 describe the full viscosity range for natural lavas.

461 **B. Effectiveness for field lava rheology and other geomaterials**

462 The typical range of mafic eruption viscosities lies within 10^1 - 10^5 Pa s (Harris and
463 Rowland, 2015 and references therein). Thus, the capable range for this penetrometer (10^2 - 10^5 Pa
464 s) fits well within the expected natural range of lava. Additionally, this penetrometer overlaps the
465 upper end of the viscosity capabilities for a field rotational viscometer, (10 - 10^4 Pa s) (Chevrel et
466 al., 2019). This means that in some settings, the penetrometer can be used in conjunction with, or,
467 in place of a field rotation viscometer to obtain rheological values of lava flows. In other instances,

468 particularly when the viscosity is intermediate to high in mafic lavas (*i.e.*, $\geq 10^4$ Pa s), like in the
469 presented field measurements, the penetrometer is currently the only instrument capable of
470 obtaining accurate *in-situ* rheological data. These characteristics support the concept of this
471 penetrometer's applicability for *in-situ* work on lava flows, and the successful deployment of this
472 device during the Iceland 2023 eruption at Litli-Hrútur served to validate the instrument's
473 capabilities.

474 The investigation of lava rheology through field measurements stands alone as the only
475 current method to investigate the properties of natural high-temperature lava. As lava cools, it
476 degasses and crystalizes until eventually, it reaches a rheological threshold where it is unable to
477 flow (Kolzenburg et al., 2019, 2020; Di Fiore et al., 2021). Currently, numerical lava-flow models
478 implement lava viscosities yet they lack field-validated values (*e.g.*, Chevrel et al., 2018b). The
479 capabilities of this new penetrometer, including portability and durability allow for accurate *in-*
480 *situ* measurements across various locations at the same lava flow. This raw field data can be used
481 to discern the rheological evolution of an effusive eruption, and thus be implemented into future
482 models that can benchmark their predictions off natural lava viscosity data. This type of work not
483 only contributes to the field of lava rheology but also has the potential to aid populations that live
484 in and around active volcanic regions and rely on rapid eruptive forecasting for their safety.

485 While the primary objective of this penetrometer device is to obtain viscosities of high-
486 temperature lavas in the field, we highlight that there are other potential applications for this
487 instrument, which may include modifying the force sensor sensitivity to match a desired viscous
488 range. Other geomaterials such as mudflows, debris flow avalanches, and snowpacks are
489 investigated for their rheological properties with penetrometers much like lava flows, to better
490 understand the risk of speed and runout distances during these hazardous events (Schneebeli and
491 Johnson, 1998; Floyer and Jamieson, 2010; Widjaja, 2019). Many of these geohazards studies rely
492 on modeling or experimental data (*e.g.*, Rognon et al., 2008; Huang and Aode, 2009; Kostynick et
493 al., 2022) and the use of our new field penetrometer on these complex heterogenous geomaterials
494 has the potential to benchmark the models and experiments to natural data obtained in the field.

495 VII. CONCLUSION

496 We present a new penetrometer device that can withstand extreme conditions such as
497 volcanic environments including high temperatures (tested to $\sim 1150^\circ\text{C}$) and corrosive gases. The

498 device is engineered with stainless steel and has self-contained electronics, all powered by a small
499 portable power bank. The device is portable and can be operated by a single person, with a length
500 of ~ 1.5 m and a weight of ~ 5.5 kg. To our knowledge, this device is the first of its kind to have
501 high-temperature resistivity, simultaneous force and displacement data acquisition, and a
502 calibrated range of data acquisition from 10^2 - 10^5 Pa s. The penetrometer's durability and effective
503 measurement range make it ideal for *in-situ* lava viscosity studies. We demonstrate that this
504 penetrometer is effective for field measurements through its use during the 2023 Litli-Hrútur
505 eruption in Iceland. Here, the penetrometer recorded the *in-situ* rheology of lavas from 1.2×10^4 to
506 3.4×10^4 (Pa s) viscosities at temperatures from 1148-1152 °C. The continued use of this instrument
507 at future eruptions will provide the necessary data that is currently lacking to better understand the
508 rheology of natural multiphase lava.

509

510 VIII. SUPPLEMENTARY MATERIAL

511 Three supplementary materials (S) accompany this manuscript.

512 S1: Penetrometer Parts and Data Acquisition Process

513 S2: Analog Material Viscosities, Measured, Known, and Calibrated

514 S3: Buoyancy Effects

515 S4: Example of Moving Averages of Penetration within Heterogenous Lava

516 S5: Geochemistry of Iceland Lava

517 IX. AUTHOR CONTRIBUTIONS

518 M.A. Harris and S. Kolzenburg conceptualized the apparatus design, geometry, and measurement
519 principle. Additionally, M.A. Harris created the data acquisition chain, engineered the electronics
520 and software, performed tests and calibrations, and led the formation of the article. I. Sonder
521 assisted with data acquisition development and data analysis. M.O. Chevrel and M.A. Harris
522 conducted field measurements in Iceland. S. Kolzenburg and M.O. Chevrel supervised and guided
523 interpretations of the instrument rheological data. All authors contributed to the writing of the
524 article.

525 X. ACKNOWLEDGMENTS

526 We thank Dr. Thorvaldur Thordarson, Dr. Ármann Höskuldsson, Dr. William Mooreland, and
527 Méline Payet—Clerc of the University of Iceland for their generous support during the field
528 measurements done during the Litli-Hrútur eruption. A special thanks to Kevin Cullinan and
529 Thomas Brachmann of the University at Buffalo Instrument Machine Shop for their countless
530 hours of work on developing the customized parts used in the penetrometer device. We are
531 indebted to Travis Parsons for his crucial help with the logistics of assembly, transport, and use of
532 the penetrometer throughout its creation, testing, and field use.

533 XI. FUNDING

534 Funding for the high-temperature tests at UB and fieldwork in Iceland was provided by the UB
535 geohazards center and NSF EAR RAPID Award No. 2241489. This project also received support
536 from NSF EAR Award No. 2223098, the Institut de Recherche pour le Développement (IRD), and
537 the French Government Laboratory of Excellence Initiative No. ANR-10-LABX-0006. This is a
538 Laboratory of Excellence ClerVolc Contribution No. xxx.

539

540 XII. DATA AVAILABILITY

541 All data that support the findings of this study are available upon the request of the
542 corresponding author. The software is openly available at
543 https://github.com/LAVAPUBMH/Lava_Field_Penetrometer

544

545 XIII. REFERENCES

546 Alidibirov, M., and Dingwell, D.B., 1996, Magma fragmentation by rapid decompression:
547 *Nature*, v. 380, p. 146–148, doi:10.1038/380146a0.

548 Avard, G., and Whittington, A.G., 2012, Rheology of arc dacite lavas: Experimental
549 determination at low strain rates: *Bulletin of Volcanology*, v. 74, p. 1039–1056,
550 doi:10.1007/s00445-012-0584-2.

551 Belousov, A., and Belousova, M., 2018, Dynamics and viscosity of ‘a’ and pahoehoe lava flows

- 552 of the 2012–2013 eruption of Tolbachik volcano, Kamchatka (Russia): *Bulletin of*
553 *Volcanology*, v. 80, doi:10.1007/s00445-017-1180-2.
- 554 Boutet, M., Dore, G., Bilodeau, J.P., and Pierre, P., 2011, Development of models for the
555 interpretation of the dynamic cone penetrometer data: *International Journal of Pavement*
556 *Engineering*, v. 12, p. 201–214, doi:10.1080/10298436.2010.488727.
- 557 Cashman, K. V, Soule, S.A., Mackey, B.H., Deligne, N.I., Deardorff, N.D., and Dietterich, H.R.,
558 2013, How lava flows: New insights from applications of lidar technologies to lava flow
559 studies: *Geosphere*, v. 9, p. 1664–1680, doi:10.1130/GES00706.1.
- 560 Chevrel, M.O., Cimarelli, C., DeBiasi, L., Hanson, J.B., Lavallée, Y., Arzilli, F., and Dingwell,
561 D.B., 2015, Viscosity measurements of crystallizing andesite from Tungurahua volcano
562 (Ecuador): *Geochemistry Geophysics Geosystems*, p. 1–20, doi:10.1002/2014GC005661.
- 563 Chevrel, M.O., Harris, A.J.L., James, M.R., Calabrò, L., Gurioli, L., and Pinkerton, H., 2018a,
564 The viscosity of pāhoehoe lava: In situ syn-eruptive measurements from Kilauea, Hawaii:
565 *Earth and Planetary Science Letters*, v. 493, p. 161–171,
566 doi:<https://doi.org/10.1016/j.epsl.2018.04.028>.
- 567 Chevrel, M.O., Labroquère, J., Harris, A.J.L., and Rowland, S.K., 2018b, PyFLOWGO: An
568 open-source platform for simulation of channelized lava thermo-rheological properties:
569 *Computers and Geosciences*, v. 111, p. 167–180, doi:10.1016/j.cageo.2017.11.009.
- 570 Chevrel, M.O., Latchimy, T., Batier, L., Delpoux, R., Harris, M.A., and Kolzenburg, S., 2023, A
571 new portable field rotational viscometer for high-temperature melts: *Review of Scientific*
572 *Instruments*, v. 94, doi:<https://doi.org/10.1063/5.0160247>.
- 573 Chevrel, M.O., Pinkerton, H., and Harris, A.J.L., 2019, Measuring the viscosity of lava in the
574 field: A review: *Earth-Science Reviews*, v. 196, doi:10.1016/j.earscirev.2019.04.024.
- 575 Dobson, K.J. et al., 2020, Quantifying Microstructural Evolution in Moving Magma: *Frontiers in*
576 *Earth Science*, v. 8, p. 1–22, doi:10.3389/feart.2020.00287.
- 577 Dubbelboer, A., Janssen, J.J.M., Zondervan, E., and Meuldijk, J., 2018, Steady state analysis of
578 structured liquids in a penetrometer: *Journal of Food Engineering*, v. 218, p. 50–60,
579 doi:10.1016/j.jfoodeng.2017.09.002.

- 580 Einarsson, T., 1949, Rate of Production of Material During the Eruption: The Flowing Lava:
581 Studies of Its Main Physical and Chemical Properties: *Societas Scientarium Islandica*, v. 4.
- 582 Einarsson, T., 1966, Studies of temperature, viscosity, density and some types of materials
583 produced in the Surtsey eruption: *Surtsey Res Program Report*, v. 1, p. 163–179.
- 584 Di Fiore, F., Vona, A., Kolzenburg, S., Mollo, S., and Romano, C., 2021, An Extended
585 Rheological Map of Pāhoehoe—‘A‘ā Transition: *Journal of Geophysical Research: Solid*
586 *Earth*, v. 126, p. 1–23, doi:10.1029/2021JB022035.
- 587 Floyer, J.A., and Jamieson, B.J., 2010, Rate-effect experiments on round-tipped penetrometer
588 insertion into uniform snow: *Journal of Glaciology*, v. 56, p. 664–672,
589 doi:10.3189/002214310793146322.
- 590 Fulcher, G.S., 1925, Analysis of recent measurements of the viscosity of glasses: *Journal of*
591 *American Ceramic Society*, v. 8.
- 592 Gauthier, F., 1973, Field and Laboratory Studies of the Rheology of Mount Etna Lava:
593 *Philosophical Transactions of the Royal Society A: Mathematical, Physical and Engineering*
594 *Sciences*, v. 274, p. 83–98.
- 595 Giordano, D., and Dingwell, D.B., 2003, Viscosity of hydrous Etna basalt: Implications for
596 Plinian-style basaltic eruptions: *Bulletin of Volcanology*, v. 65, p. 8–14,
597 doi:10.1007/s00445-002-0233-2.
- 598 Giordano, D., Russell, J.K., and Dingwell, D.B., 2008, Viscosity of magmatic liquids: A model:
599 *Earth and Planetary Science Letters*, v. 271, p. 123–134, doi:10.1016/j.epsl.2008.03.038.
- 600 Hall, R., Stumpf, A., Baji, A., Ross, R., and Barnett, D., 2022, Characterising Penetrometer Tip
601 Contact during Concrete Condition Assessment: *Sensors*, v. 22, p. 1–12,
602 doi:10.3390/s22030737.
- 603 Harris, C.R. et al., 2020, Array programming with NumPy: *Nature*, v. 585, p. 357–362,
604 doi:10.1038/s41586-020-2649-2.
- 605 Harris, A.J., and Allen, J.S., 2008, One-, two- and three-phase viscosity treatments for basaltic
606 lava flows: *Journal of Geophysical Research*, v. 113, doi:10.1029/2007JB005035.

- 607 Harris, A.J.L., and Rowland, S.K., 2015, Lava Flows and Rheology: Elsevier Inc., 321–342 p.,
608 doi:10.1016/b978-0-12-385938-9.00017-1.
- 609 Heap, M.J., Xu, T., and Chen, C., 2014, The influence of porosity and vesicle size on the brittle
610 strength of volcanic rocks and magma: *Bulletin of Volcanology*, v. 76, p. 1–15,
611 doi:10.1007/s00445-014-0856-0.
- 612 Herrick, J.E., and Jones, T.L., 2002, A dynamic cone penetrometer for measuring soil
613 penetration resistance: *Soil Science Society of America Journal*, v. 66, p. 1320–1324,
614 doi:10.2136/sssaj2002.1320.
- 615 Hess, K.U., Cordonnier, B., Laval e, Y., and Dingwell, D.B., 2007, High-load, high-temperature
616 deformation apparatus for synthetic and natural silicate melts: *Review of Scientific
617 Instruments*, v. 78, doi:10.1063/1.2751398.
- 618 Hess, K.U., and Dingwell, D.B., 1996, Viscosities of hydrous leucogranitic melts: a non-
619 Arrhenian model: *American Mineralogist*, v. 81, p. 1297–1300.
- 620 Hobiger, M., Sonder, I., B uttner, R., and Zimanowski, B., 2011, Viscosity characteristics of
621 selected volcanic rock melts: *Journal of Volcanology and Geothermal Research*, v. 200, p.
622 27–34, doi:10.1016/j.jvolgeores.2010.11.020.
- 623 Hon, K., Gansecki, C., and Kauahikaua, J., 2003, The transition from 'A' a to p ahoehoe crust on
624 flows emplaced during the Pu'u 'O' o-K upaianaha eruption: *US Geological Survey
625 Professional Paper*, p. 89–103.
- 626 Huang, Z., and Aode, H., 2009, A laboratory study of rheological properties of mudflows in
627 Hangzhou Bay, China: *International Journal of Sediment Research*, v. 24, p. 410–424,
628 doi:10.1016/S1001-6279(10)60014-5.
- 629 Hunter, J.D., 2007, Matplotlib: A 2D Graphics Environment: *Computing in Science and
630 Engineering*, v. 9, p. 90–95, doi:10.1109/MCSE.2007.55.
- 631 Jantra, C., Slaughter, D.C., Roach, J., and Pathaveerat, S., 2018, Development of a handheld
632 precision penetrometer system for fruit firmness measurement: *Postharvest Biology and
633 Technology*, v. 144, p. 1–8, doi:<https://doi.org/10.1016/j.postharvbio.2018.05.009>.

- 634 Kauahikaua, J., Sherrod, D.R., Cashman, K. V., Heliker, C., Hon, K., Mattox, T.N., and Johnson,
635 J.A., 2003, Hawaiian lava-flow dynamics during the Pu'u 'Ō'ō-Kū paianaha eruption: A
636 tale of two decades: US Geological Survey Professional Paper, p. 63–87.
- 637 Keszthelyi, L.P., 1994, On the Thermal Budget of Pahoehoe Lava Flows: California Institute of
638 Technology, 274 p.
- 639 Kirkham, M.B., 2014, Chapter 11 - Penetrometers, *in* Kirkham, M.B.B.T.-P. of S. and P.W.R.
640 (Second E. ed., Principles of Soil and Plant Water Relations, Boston, Academic Press, p.
641 171–183, doi:<https://doi.org/10.1016/B978-0-12-420022-7.00011-2>.
- 642 Kolzenburg, S., Chevrel, M.O., and Dingwell, D.B., 2022, Magma / Suspension Rheology:
643 Reviews in Mineralogy and Geochemistry, v. 87, p. 639–720, doi:10.2138/rmg.2022.87.14.
- 644 Kolzenburg, S., Giordano, D., Di Muro, A., and Dingwell, D.B., 2019, Equilibrium viscosity and
645 disequilibrium rheology of a high magnesium basalt from piton de la fournaise volcano, la
646 reunion, indian ocean, France: Annals of Geophysics, v. 62, doi:10.4401/ag-7839.
- 647 Kolzenburg, S., Hess, K.-U., Berlo, K., and Dingwell, D.B., 2020, Disequilibrium Rheology and
648 Crystallization Kinetics of Basalts and Implications for the Phlegrean Volcanic District:
649 Frontiers in Earth Science, v. 8, doi:10.3389/feart.2020.00187.
- 650 Kostynick, R., Matinpour, H., Pradeep, S., Haber, S., Sauret, A., Meiburg, E., Dunne, T., Arratia,
651 P., and Jerolmack, D., 2022, Rheology of debris flow materials is controlled by the distance
652 from jamming: Proceedings of the National Academy of Sciences of the United States of
653 America, v. 119, p. 1–10, doi:10.1073/pnas.2209109119.
- 654 Llewellyn, E.W., Mader, H.M., and Wilson, S.D.R., 2002, The constitutive equation and flow
655 dynamics of bubbly magmas: Geophysical Research Letters, v. 29, p. 1–4,
656 doi:10.1029/2002GL015697.
- 657 Macosko, C.W., 1994, Rheology: Principles, Measurements and Applications, p. 1–576,
658 [https://app.knovel.com/hotlink/pdf/id:kt0059EKWM/rheology-principles-](https://app.knovel.com/hotlink/pdf/id:kt0059EKWM/rheology-principles-measurements/part-i-constitutive-relations)
659 [measurements/part-i-constitutive-relations](https://app.knovel.com/hotlink/pdf/id:kt0059EKWM/rheology-principles-measurements/part-i-constitutive-relations).
- 660 Mader, H.M., Llewellyn, E.W., and Mueller, S.P., 2013, The rheology of two-phase magmas: A
661 review and analysis: Journal of Volcanology and Geothermal Research, v. 257, p. 135–158,

662 doi:10.1016/j.jvolgeores.2013.02.014.

663 Marsh, B.D., 1981, On the crystallinity, probability of occurrence, and rheology of lava and
664 magma: *Contributions to Mineralogy and Petrology*, v. 78, p. 85–98,
665 doi:10.1007/BF00371146.

666 Moitra, P., and Gonnermann, H.M., 2015, Effects of crystal shape- and size-modality on magma
667 rheology: *Geochemistry, Geophysics, Geosystems*, v. 16, p. 1–26,
668 doi:10.1002/2014GC005554.

669 De Moraes, M.T., Da Silva, V.R., Zwirtes, A.L., and Carlesso, R., 2014, Use of penetrometers in
670 agriculture: A review: *Engenharia Agricola*, v. 34, p. 179–193, doi:10.1590/S0100-
671 69162014000100019.

672 Panov, V.K., Slezin, Yu. B, and Storcheus, A.V, 1988, Mechanical Properties of Lava Extruded
673 in 1983 Predskazannyi Eruption (Klyuchevskoi Volcano): *Journal of Volcanol Seismol*, v.
674 7, p. 25–37.

675 Pinkerton, H., 1978, *Methods of measuring the rheological properties of lava.*: Ph.D. Lancaster.

676 Pinkerton, H., Herd, R.A., Kent, R.M., and Wilson, L., 1995a, Field Measurements of the
677 Rheological Properties of Basaltic Lavas, *in* *Abstracts of the Lunar and Planetary Science*
678 *Conference*, p. 1127–1128.

679 Pinkerton, H., and Norton, G., 1995, Rheological properties of basaltic lavas at sub-liquidus
680 temperatures: laboratory and field measurements on lavas from Mount Etna: *Journal of*
681 *Volcanology and Geothermal Research*, v. 68, p. 307–323, doi:10.1016/0377-
682 0273(95)00018-7.

683 Pinkerton, H., Norton, G.E., Dawson, J.B., and Pyle, D.M., 1995b, Field Observations and
684 Measurements of the Physical Properties of Oldoinyo Lengai Alkali Carbonatite Lavas,
685 November 1988 BT - Carbonatite Volcanism: Oldoinyo Lengai and the Petrogenesis of
686 Natrocarbonatites, *in* Bell, K. and Keller, J. eds., Berlin, Heidelberg, Springer Berlin
687 Heidelberg, p. 23–36, doi:10.1007/978-3-642-79182-6_3.

688 Pinkerton, H., and Sparks, R.S.J., 1978, Field measurements of the rheology of lava: *Nature*, v.
689 276, p. 383–385, doi:10.1038/276383a0.

- 690 Pinkerton, H., and Stevenson, R.J., 1992, Methods of determining the rheological properties of
691 magmas at sub-liquidus temperatures: *Journal of Volcanology and Geothermal Research*, v.
692 53, p. 47–66, doi:10.1016/0377-0273(92)90073-M.
- 693 Pistone, M., Caricchi, L., Ulmer, P., Reusser, E., and Ardia, P., 2013, Rheology of volatile-
694 bearing crystal mushes: Mobilization vs. viscous death: *Chemical Geology*, v. 345, p. 16–
695 39, doi:10.1016/j.chemgeo.2013.02.007.
- 696 Robert, B., Harris, A., Gurioli, L., Médard, E., Sehlke, A., and Whittington, A., 2014, Textural
697 and rheological evolution of basalt flowing down a lava channel: *Bulletin of Volcanology*,
698 v. 76, p. 1–21, doi:10.1007/s00445-014-0824-8.
- 699 Rognon, P.G., Chevoir, F., Bellot, H., Ousset, F., Naaïm, M., and Coussot, P., 2008, Rheology of
700 dense snow flows: Inferences from steady state chute-flow experiments: *Journal of*
701 *Rheology*, v. 52, p. 729–748, doi:10.1122/1.2897609.
- 702 Rust, A.C., and Manga, M., 2002, Effects of bubble deformation on the viscosity of dilute
703 suspensions: *Journal of Non-Newtonian Fluid Mechanics*, v. 104, p. 53–63,
704 doi:10.1016/S0377-0257(02)00013-7.
- 705 Sato, H., 2005, Viscosity measurement of subliquidus magmas: 1707 basalt of Fuji volcano:
706 *Journal of Mineralogical and Petrological Sciences*, v. 100, p. 133–142,
707 doi:10.2465/jmps.100.133.
- 708 Schneebeli, M., and Johnson, J.B., 1998, A constant-speed penetrometer for high-resolution
709 snow stratigraphy: *Annals of Glaciology*, v. 26, p. 1–5,
710 doi:<https://doi.org/10.3189/1998AoG26-1-107-111>.
- 711 Sehlke, A., Whittington, A., Robert, B., Harris, A., Gurioli, L., and Médard, E., 2014, Pahoehoe
712 to áá transition of Hawaiian lavas: An experimental study: *Bulletin of Volcanology*, v. 76,
713 doi:10.1007/s00445-014-0876-9.
- 714 Shaw, H.R., 1969, Rheology of basalt in the melting range: *Journal of Petrology*, v. 10, p. 510–
715 535, doi:10.1093/petrology/10.3.510.
- 716 Shaw, H.R., Wright, T.L., Peck, D.L., and Okamura, R., 1968, The Viscosity of Basaltic Magma:
717 An Analysis of Field Measurements in Makaopuhi Lava Lake, Hawaii: *American Journal of*

718 Science, v. 266, p. 225–264.

719 Tanaka, M., De Man, J.M., and Voisey, P.W., 1971, Measurement of textural properties of foods
720 with a constant speed cone penetrometer: *Journal of Texture Studies*, v. 2, p. 306–315,
721 doi:<https://doi.org/10.1111/j.1745-4603.1971.tb01007.x>.

722 Tanaka, M., Pearson, A.M., and deMan, J.M., 1972, Measurement of Ice Cream Texture with the
723 Constant Speed Penetrometer: *Canadian Institute of Food Science and Technology Journal*,
724 v. 5, p. 105–110, doi:[https://doi.org/10.1016/S0315-5463\(72\)74098-5](https://doi.org/10.1016/S0315-5463(72)74098-5).

725 Truby, J.M., Mueller, S.P., Llewelin, E.W., and Mader, H.M., 2015, The rheology of three-
726 phase suspensions at low bubble capillary number: *Proceedings of the Royal Society A:
727 Mathematical, Physical and Engineering Sciences*, v. 471, doi:10.1098/rspa.2014.0557.

728 Vogel, D.H., 1921, Temperaturabhängigkeitsgesetz der Viskosität von Flüssigkeiten:
729 *Physikalische Zeitschrift*, v. 22, p. 645.

730 Widjaja, B., 2019, Landslide and Mudflow Behavior Case Study in Indonesia: Rheology
731 Approach: *IPTEK Journal of Proceedings Series*, v. 0, p. 93,
732 doi:10.12962/j23546026.y2019i3.5849.

XIV. FIGURES

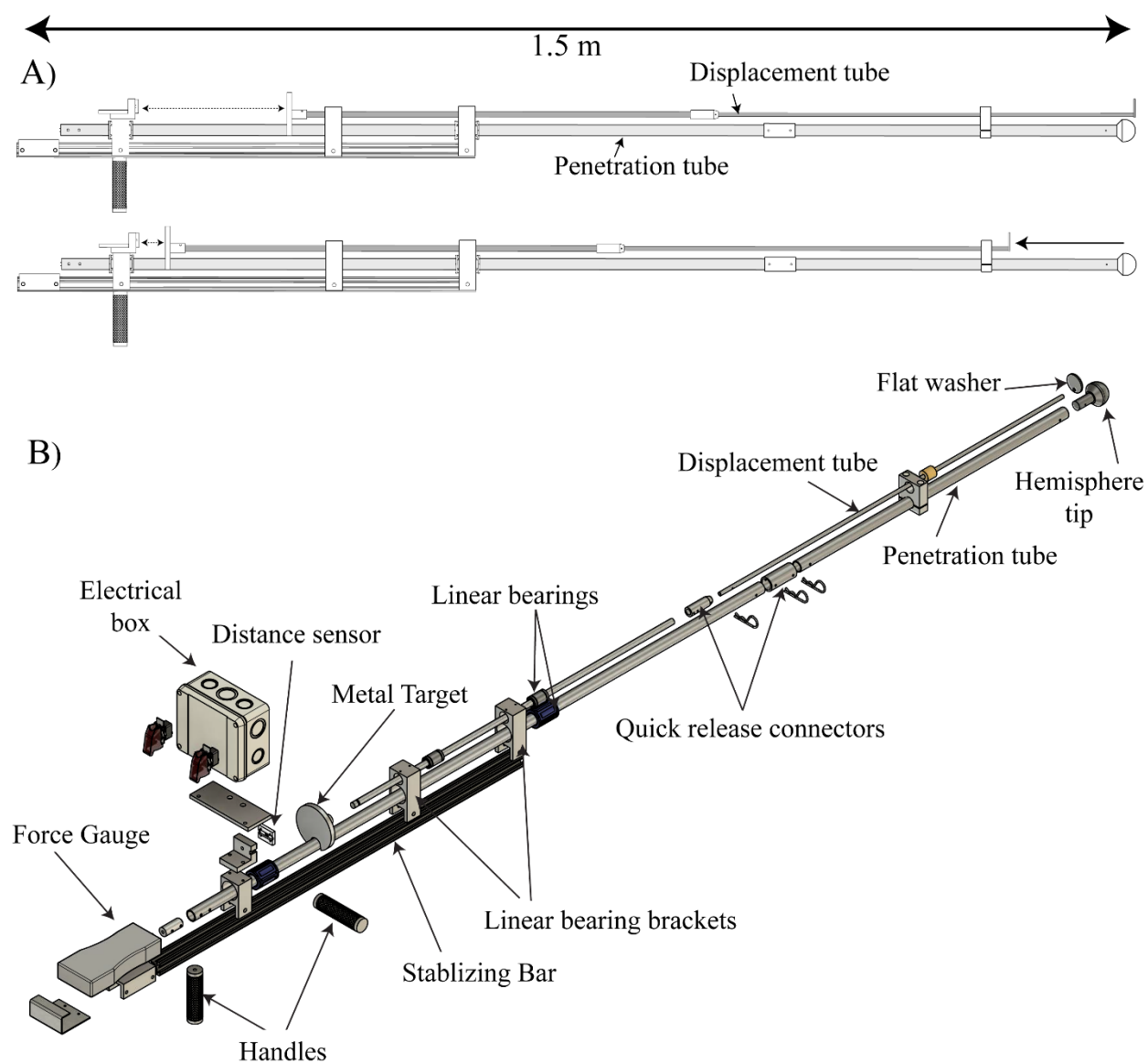


Figure 1: Computer-aided design (CAD) rendering of the new penetrometer device for rheology measurements. A) Simple profile views that highlight the two main components, 1) the penetration tube and 2) the displacement tube, with the relative motion of the displacement tube shown. B) An exploded view of the major components of the penetrometer. Drawings of all individual custom machined parts with detailed specifications can be found within

supplementary material 1. CAD image rendering done by Thomas Brachmann (UB CAS machine shop technician), at a scale of 1:7.

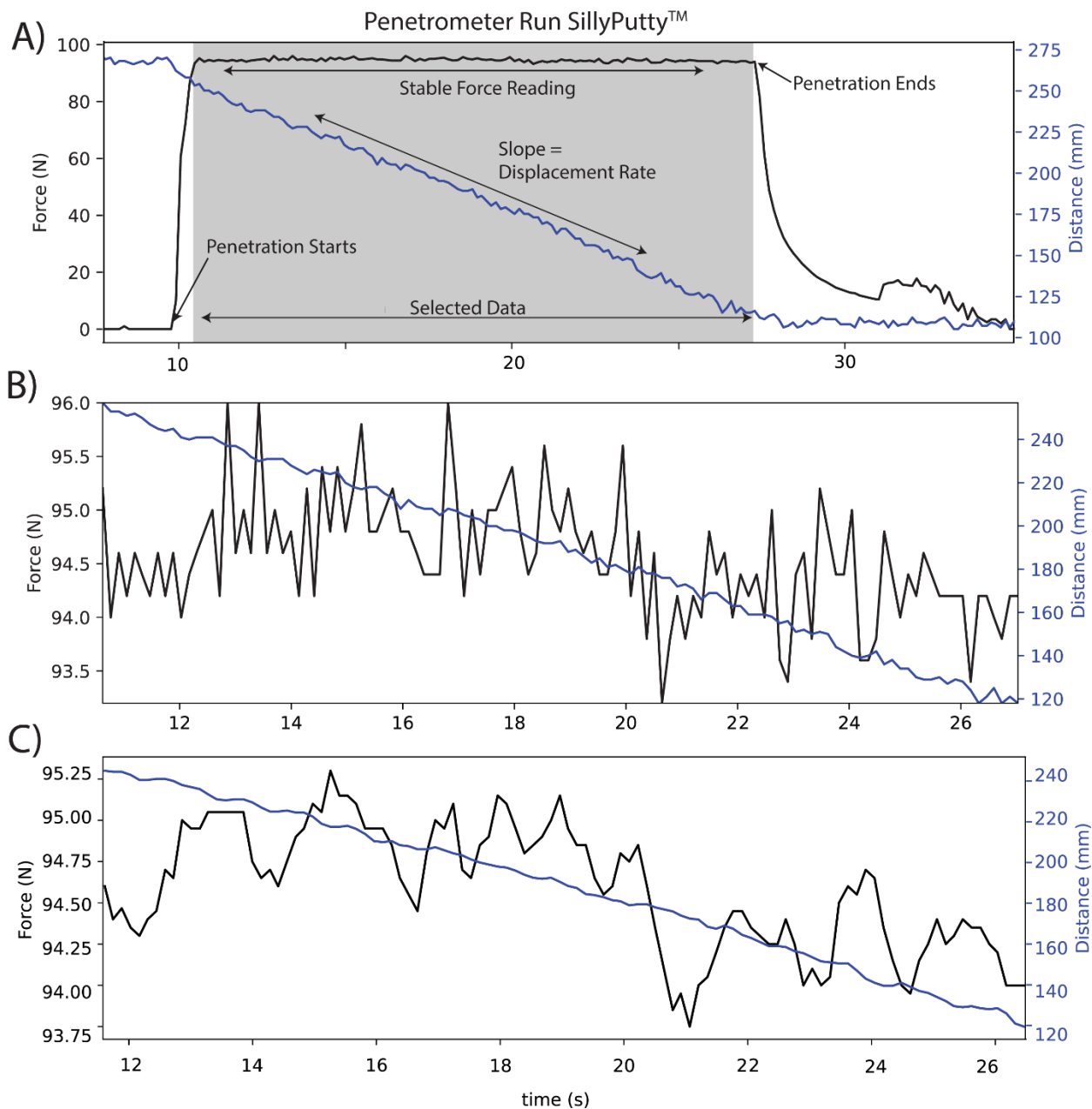


Figure 2: Examples of data recorded from penetrometer during testing with SillyPutty™. A) Full record of raw data from the output text file, with time on the x-axis, Force (N) on the y-axis (left), and displacement (mm) on the y-axis (right). The data recorded by the force gauge is shown in black and data recorded by the distance sensor is shown in blue. The grey field is the area of data selection shown in B. B) Extracted raw data from the selected portion (grey) in

subplot A. C) The data shown here is processed after a moving average function (window of five) that smooths some of the sensor noise. This data is then used to calculate the changing force with displacement (velocity) throughout the measurement. These values of force and velocity are used to calculate the viscosity of the measured material (here SillyPutty™).

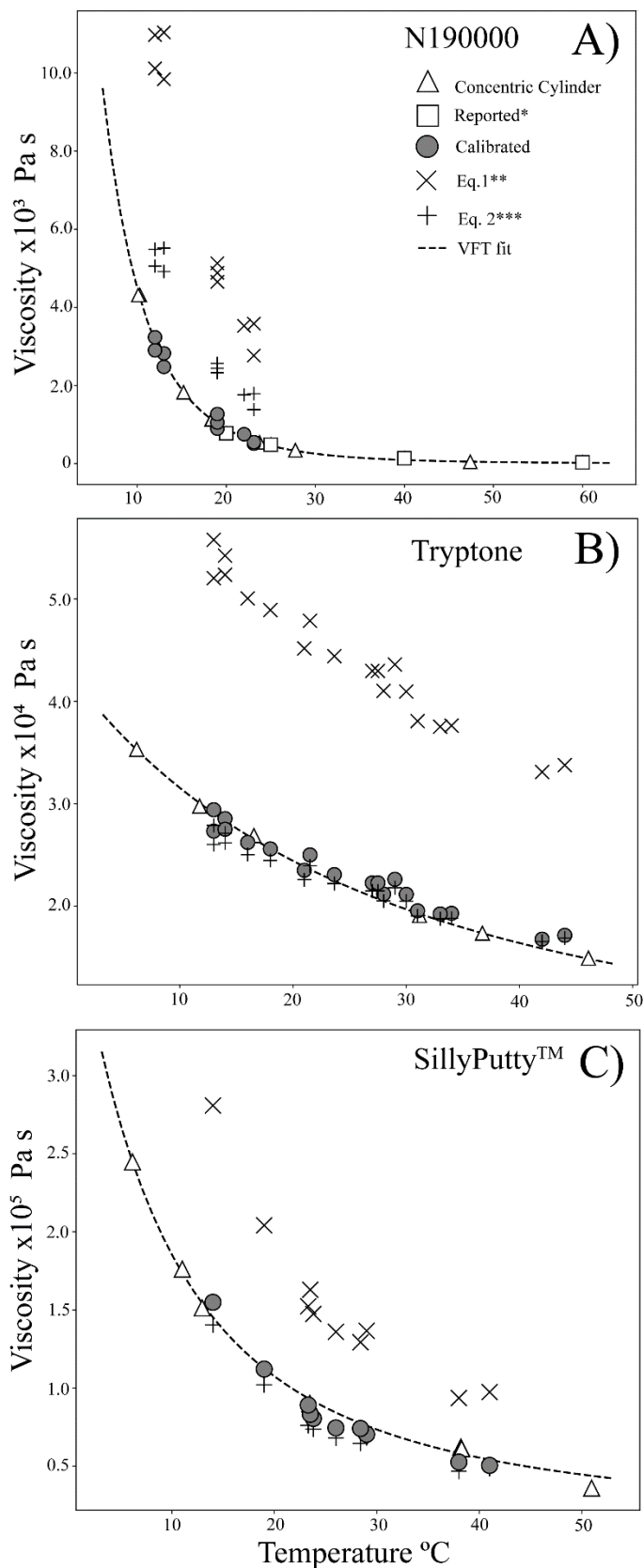


Figure 3: Plots showing the temperature-dependent viscosity of N190000 (A), Tryptone (B), and SillyPutty™ (C). The data measured with a concentric cylinder rheometer is shown with triangles and a VFT fit to the data as a dashed line. The values recovered from the penetrometer data following the calibration procedure detailed in the text are shown with grey circle symbols. * certified viscosity values for N190000 as given by Cannon®, shown as squares. **Viscosities derived from modified Stoke’s Law (Eq.1) are shown as cross symbols. ***Viscosities derived from Stoke’s Law (Eq.2) are shown as plus symbols. Individual points are larger than the uncertainty.

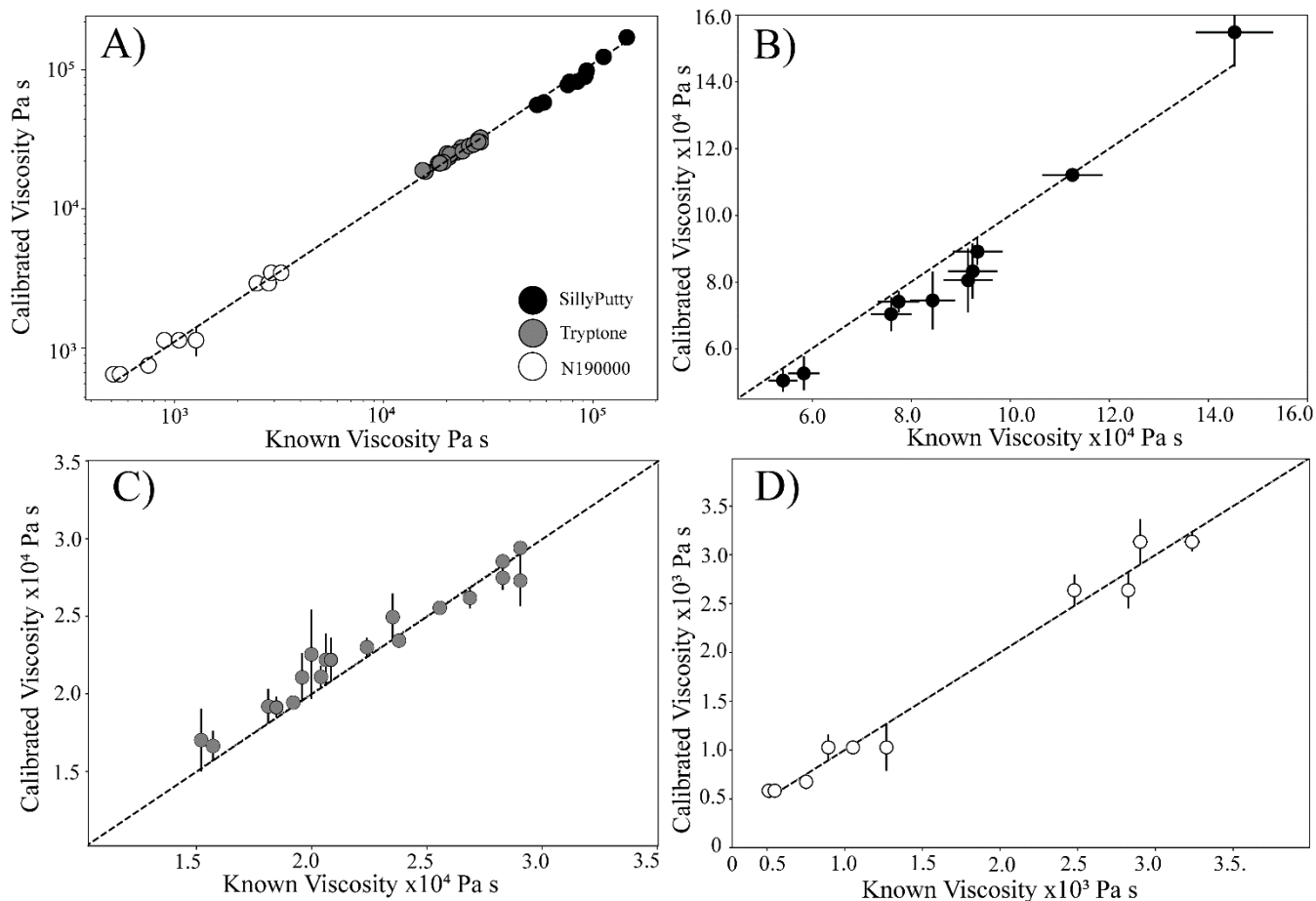


Figure 4: Plots showing measured viscosity values with the new penetrometer versus the known viscosity of the material for three different analog materials. Here the measured values are derived from the penetrometer sensor data with the calibration factors applied. The known values are from NIST traceable standards and traceable internal reference materials. A) The full range of three analog materials. B) SillyPuttyTM. C) Tryptone. D) N190000 Oil. The dashed line gives the 1:1 relationship. Error bars are 2σ .

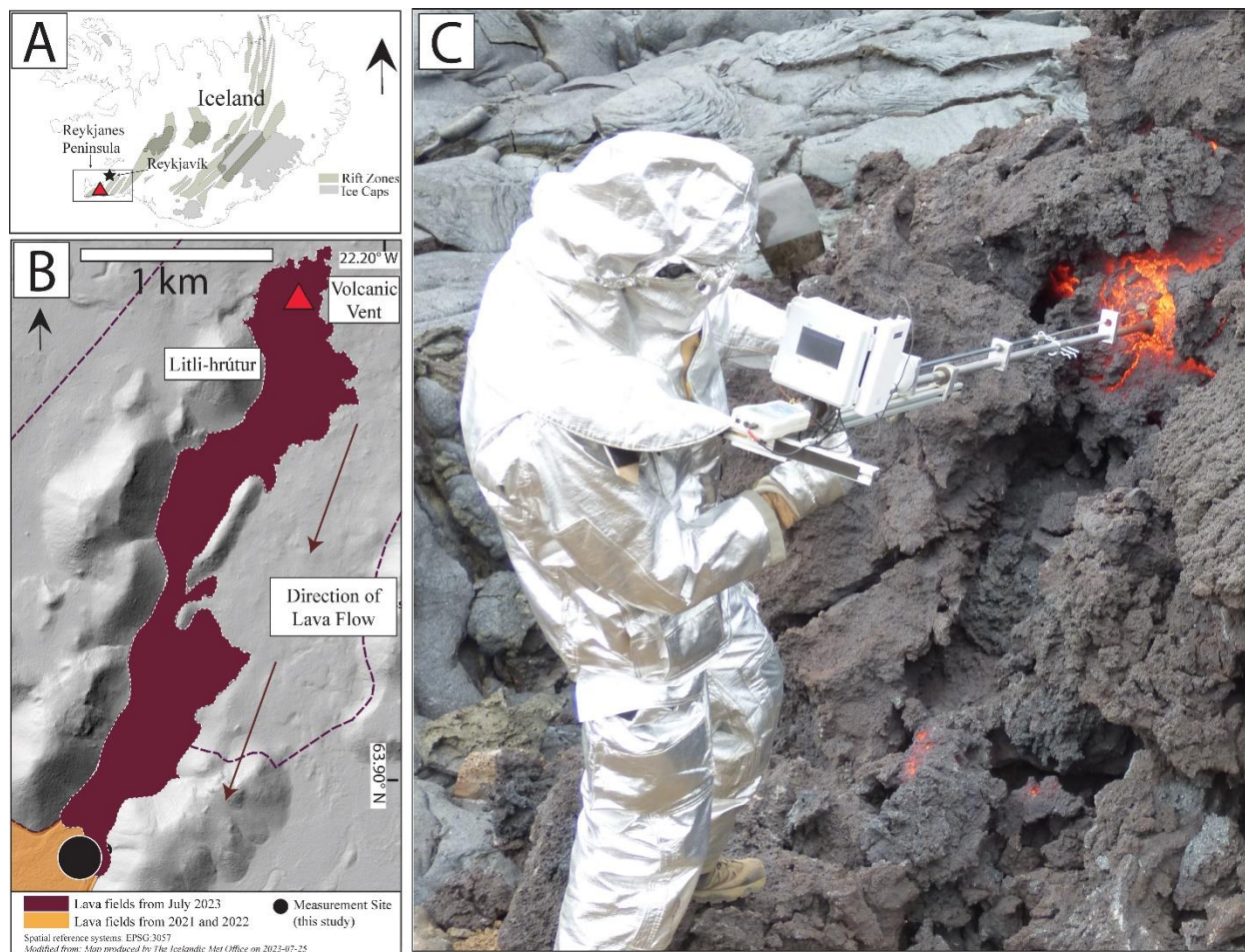


Figure 5: Map of 2023 Litli-Hrútur Eruption in Iceland and view of field usage of the penetrometer. The black vertical arrows denote North. A) Regional setting of the eruption within the southwest Reykjanes Peninsula. The red triangle denotes the vent location. Rift zones and ice caps are shown in dark and light grey, respectively. B) Map showing the extent of the lava flow field from the Litli-Hrútur eruption on July 25, 2023. C) Field usage of the penetrometer, the operator is 1.88 meters tall for scale.

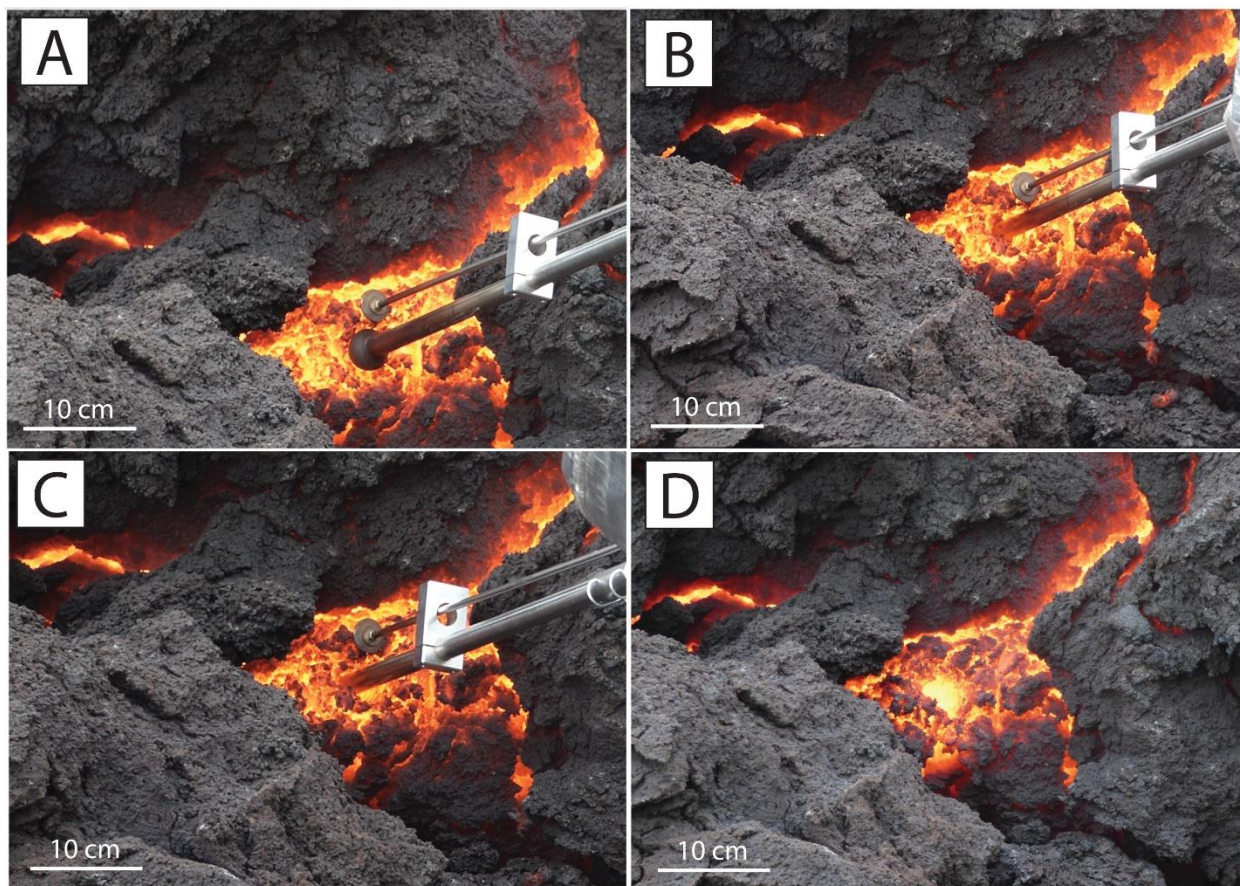


Figure 6: A close view of the progression of the lava penetrometer used in high-temperature lava. A-C) shows the progression of the hemisphere entering the lava while the displacement rod rests on the exterior crust. D) Shows the hole left in the lava after penetrometer extraction with a diameter of the penetrometer tip.

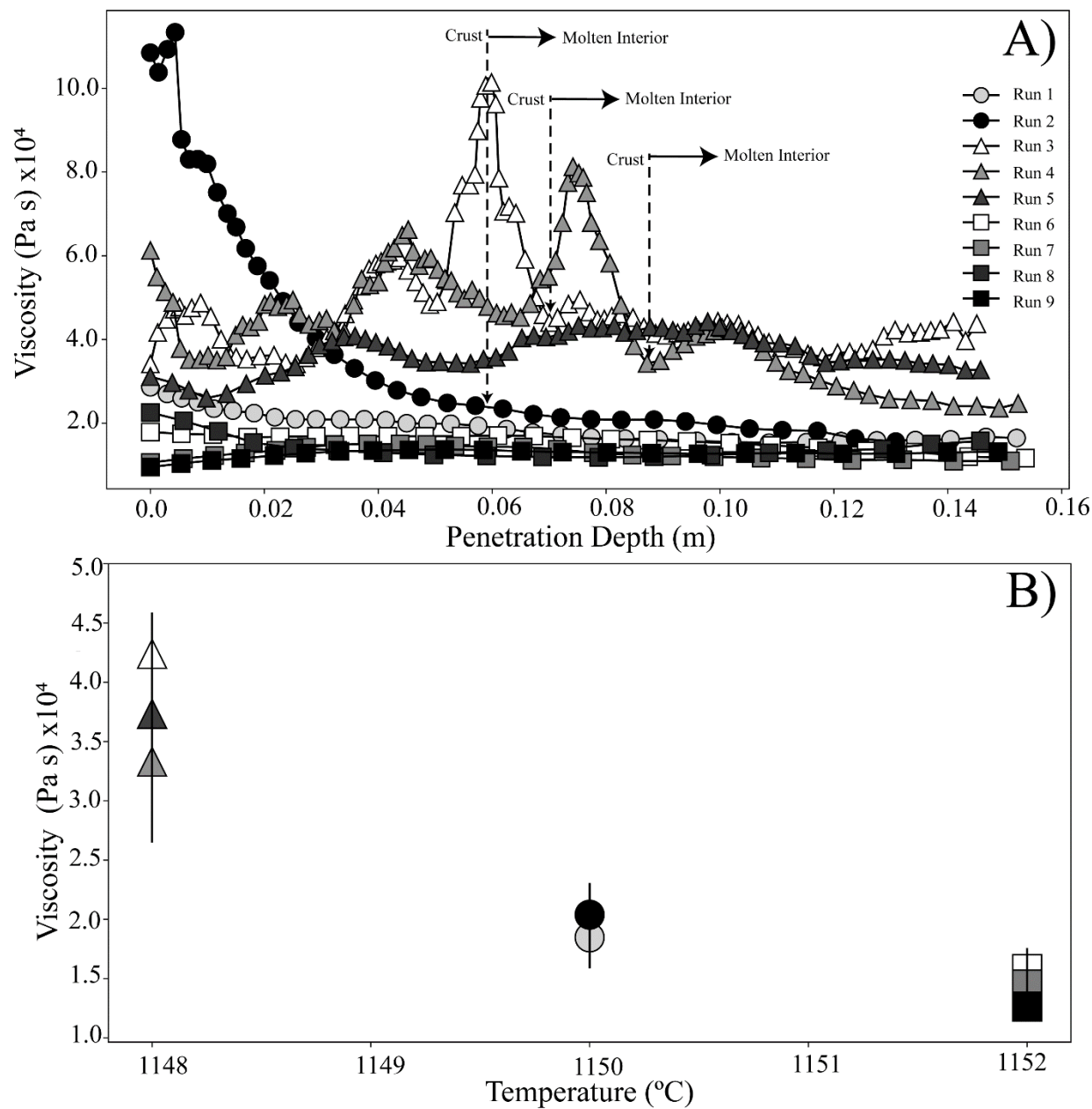


Figure 7: Plots showing the processed data from nine penetrometer measurements within lava from the Litli-Hrútur eruption at the single location shown in Figure 5. A) Measured viscosity (Pa s) versus the depth of penetration (m). The dashed line with arrow symbols indicates runs where initially high or fluctuating viscosity values are followed by a decrease and then stabilized viscosity. Data on the left of the arrow are interpreted as crustal penetration and the right of the arrow is interpreted as the molten interior. The changing viscosity profiles for Runs 2-4 display the penetrometer’s ability to capture transient rheological properties of a heterogeneous material within a single measurement. B) The viscosity (Pa s) of only the molten interior plotted against the temperature ($^{\circ}\text{C}$) of the molten interior. The data document the temperature-dependent viscosities with nearly a three-fold increase in apparent viscosity within a temperature decrease

of 4 °C. The temperatures were recovered from the same K-type thermocouple (± 1 °C) inserted into the lava adjacent to the measurement sites.